Investigation of the Benguela upwelling eddies using Lagrangian modeling methods

Tatyana V. Belonenko[1] · Maksim V. Budyansky[2] · Avelina F. Akhtyamova[1] · Alexander A. Udalov[2]

Abstract

In this research, we utilize AVISO altimetry data, the GLORYS12V1 product, and the META3.2 DT Atlas to investigate the Benguela upwelling. By combining these three datasets, we explore the propagation of mesoscale eddies generated within the upwelling zone and examine the dispersion of particles originating from the upwelling zone. The geographical scope of our analysis is confined to the region between 10–36°S and 0–20°E. We employ Lagrangian analysis and the AMEDA approach to study the eddies formed in the upwelling zone. The diverse methods applied enable us to track the movement of upwelling fluid elements in the specified area. The identification of the upwelling zone relies on temperature and salinity gradients in the coastal region. The primary focus of this study revolves around mesoscale eddies emerging in the upwelling zone. We scrutinize the trajectories of cyclones and anticyclones as they propagate westward from the upwelling zone, highlighting variations in the number of upwelling-origin particles within these eddies. We observe distinctions in the locations of upwelling cells between cyclones and anticyclones. Our results indicate that among mesoscale eddies generated in the upwelling zone cyclones predominate. We show that Lagrangian particles, leaving the upwelling zone, propagate throughout the area under consideration. For these particles, we can determine the travel time from the upwelling zone from 1 to 365 days and distances of 500 km for cyclones and 300 km for anticyclones. We found that cyclones are more stable structures with a longer lifetime and with a longer distance traveled in contrast to anticyclones. We believe this is a distinctive feature of the eddies with upwelling origins in comparison with other mesoscale eddies in the area. Finally, we analyze the change of water properties inside the eddies after they leave the upwelling zone and show a significant renewal of vortex cores occurring after 1–2 months of their life.

Keywords Benguela upwelling · Mesoscale eddies · Altimetry · GLORYS12V1 · META3.2 · Lagrangian analysis · AMEDA

1 Introduction

Various texts offer diverse interpretations of the term "upwelling". Let's take a brief look at a few of these definitions. 1. Upwelling is the phenomenon of colder, saltier, and biogeochemically enriched deep waters rising to the surface (Sangrà et al. 2009). 2. Upwelling is a persistently existing region of uplift of deep waters in the ocean, associated with dynamically evolving and distinctly periodic events in the coastal zone (Woodson et al. 2007). 3. Upwelling is the result of Ekman transport in the coastal zone during alongshore winds, offshore wind stress during onshore winds (Svansson 1975), alongshore currents (Walin 1972), and the passage of Kelvin waves (Fennel and Seifert 1995).

The rising of cold waters during upwelling locally affects the weather, influencing the atmospheric phenomena observed in a specific area. Weather conditions in coastal areas adjacent to upwelling regions are marked by fog, a slight and low stratiform cloud cover, stable atmospheric stratification, and weak convection (Stewart 2006). The occurrence of upwelling phenomena can be deduced from anomalies in sea surface temperature. Winds drive warm surface water away from the coast, enabling cold,

✉ Tatyana V. Belonenko
btvlisab@yandex.ru

1   St. Petersburg State University, Universitetskaya nab,
    St. Petersburg 199034, Russia

2   Pacific Oceanological Institute, Russian Academy
    of Sciences, 43 Baltiiskaya St, 690041 Vladivostok, Russia

nutrient-rich water to ascend from the depths, enriched with dissolved substances such as oxygen, nitrates, and other abiotic compounds (Stewart 2006). Chlorophyll concentration is a crucial parameter that indicates the condition of ocean water, reflecting the abundance of phytoplankton – single-celled plants that inhabit nutrient-rich upwelling waters. The presence of phytoplankton attracts zooplankton, which then becomes a food source for a significant number of fish and other marine organisms. Consequently, coastal areas influenced by upwelling, owing to the substantial supply of biogeochemical elements to the surface, serve as highly productive fishing grounds, contributing to more than half of the world's catch (Chernyshkov et al. 2005).

The Benguela upwelling region is situated in the Southeast Atlantic, with boundaries defined by The Food and Agriculture Organization of the United Nations (FAO, https://www.fao.org) as 6–50°S and 20°W–30°E. This study focuses on the waters adjacent to the southwest coast of Africa within the range of 10°–36°S and 0°–20°E, as this is where upwelling is most intense. Seasonal and interannual variations in large-scale oceanographic and biological processes in this region are largely connected to changes in the wind field, which, in turn, depend on the rearrangement of the atmospheric pressure field throughout the year. The prevailing southeast trade winds in the Benguela upwelling region, accounting for more than 80% stability, result from the atmospheric pressure gradient between the South Atlantic Anticyclone (a high-pressure oceanic area in the South Atlantic) and the Equatorial Depression (a low-pressure zone near the equator) extending southward over the African continent. The wind direction undergoes seasonal variations, ranging from east to southwest, with a predominance of south and southeast winds averaging speeds of 6–12 m/s.

The majority of significant and seasonal coastal upwelling systems are formed by winds blowing parallel to the coastline, resulting in Ekman transport. When persistent winds move across the ocean surface, they create an Ekman layer that displaces water to the left (in the southern hemisphere) of the wind direction. Consequently, any spatial variations in the wind field over the open ocean can induce either upwelling or downwelling (Stewart 2006). The presence of strong winds in the Benguela upwelling region is typically linked to two primary types of synoptic situations. In one scenario, preceding the arrival of an anticyclone to the continent, there is an increase in pressure at its center, accompanied by a relatively rapid rise in baric gradients on its northeastern periphery. In the other scenario, baric gradients become more pronounced on the northern periphery of the anticyclone as its center approaches the continent. Some researchers propose that in the Benguela upwelling zone, unlike in temperate latitudes, the occurrence of strong winds is not linked to active cyclonic activity but rather to

the evolution of the subtropical anticyclone itself (Chernyshkov et al. 2005).

Winds blowing parallel to the coast in a northward direction are responsible for the formation of the Benguela current. The Benguela current is predominantly a surface flow but can extend to depths of up to 800–1000 meters in certain locations. The estimated width of the Benguela current is approximately 100 miles (Wysokinski 1986; Shannon 2001). The velocity of the Benguela current exhibits significant variation, typically falling within the range of 25–50 cm/s.

The Benguela current is among the eastern boundary currents associated with subtropical anticyclonic circulation, centered around 33°S, 10°W. It encompasses scattered eastern branches of the subtropical gyre, exhibiting a northward transport of approximately 23 Sv, while the westward branch is estimated to have a transport of 17 Sv (Neiman 1973). The Benguela current system, composed of various branches, including a narrow coastal current and a broader offshore flow, extends roughly from the Agulhas Ridge in the south to around 16°S, with extensions observed at around 12–13°S and further north (Shannon 1985). The Benguela Current is flanked by warm water masses, specifically the Angola Current to the north and the Agulhas Current to the south. The interaction between the Benguela current and these currents extends meridionally for up to 1000 km (Shannon 1985). The oceanic thermal front in the southern part of the region is closer to the coast compared to the northern part (Shannon 1985). A well-defined frontal zone between the Angola and Benguela currents extends from east to west off the African coast, reaching approximately 150 km offshore along the parallel of 16°S. The zone of maximum gradients near the coast is shifted over the waters between 15°S and 17°S, typically positioned north and south in August and March, respectively (Shannon 1985, 2001). The demarcation between the two currents is most evident in the upper 0–75 meters layer, although the vertical distribution of salinity across the frontal zone suggests that the front can extend to depths of several hundred meters (Shannon 1985). Satellite and ship observations of surface temperature reveal the existence of a wavelike front in the north, with its distinctive features closely associated with the configuration of the continental shelf break and the upwelling center. During certain periods, extensive tongues of cool water masses extend westward into the open ocean, reaching distances up to 500 km or more, particularly around 26–27°S. This significant westward displacement of the front is also observable in the thermohaline structure of water masses at a depth of 400 m near Lüderitz. The frontal structure in the southern part of the Benguela system seems to be more intense, marked by more pronounced gradients compared to the northern part. In the southern part, there is the presence of a jet-like

frontal system at the shelf edge, and similar jet-like currents are evident in the central and northern parts of the Benguela system. Beneath the surface layer across much of the shelf in the Benguela current system, a southward transport system is evident, as indicated by dynamic calculations of currents along latitudinal sections. West of the shelf break in most of the region, there is a subsurface flow directed poleward (deep compensating flow). This phenomenon is particularly pronounced in the region north of 25°S (Shannon 1985; Chernyshkov et al. 2005).

The southern and southeast trade winds play a significant role in generating an exceptionally strong upwelling along the southwest coast of Africa. These winds displace the surface waters away from the coast, creating a vacuum-like effect that draws nutrient-rich waters from below. The upwelling processes unfold as follows: in the narrow coastal zone, against the backdrop of relatively cold waters, centers of outflow of the coldest upwelled waters are observed. These are referred to as local coastal upwelling spots or upwelling cells (Shannon 1985, 2001; Chernyshkov et al. 2005). The development of these cells is linked to the seabed's topography and the configuration of the coastline. In a broader zone, within a distance of 200–300 kilometers from the shore, a patchy structure of water can also be observed, evident in satellite images. The spatial distribution of upwelling cells has been thoroughly examined in the study conducted by Lutjeharms and Meeuwis (1987).

Fluctuations in the ecosystem of the southern part of the Benguela upwelling system result in regular replenishment of nutrient stocks during active upwelling and phytoplankton blooms when the winds weaken (Pavlushin and Kubryakov 2022). However, according to some studies, there may not be a direct relationship between the presence of "favorable" winds and the occurrence of coastal upwelling. Upwelling can occur with winds of different directions or even in their absence (Kahru et al. 1995; Woodson et al. 2007). Thus, there are factors influencing upwelling beyond the direct impact of winds. The Benguela upwelling is most intense in July and weakens in April. Temperature and salinity anomalies in the 100–600 m layer during this time reach 0.5°C and 0.05 psu, respectively. A secondary maximum of upwelling is observed in January in the 0–400 m layer, and a secondary minimum occurs in December. On interannual scales, two periods of significant upwelling weakening were recorded in 2004–2005 and 2018–2019 (Pavlushin and Kubryakov 2022).

The Benguela upwelling system exhibits high dynamic activity across various spatial and temporal scales (Manta et al. 2021; Ioannou et al. 2022). The synergistic impact of robust Ekman transport of surface waters and the upwelling of subsurface waters along the coast triggers barotropic and baroclinic instabilities in the currents, resulting in the formation of mesoscale eddies in the upwelling region (Pegliasco et al. 2015).

It is well-established that Agulhas rings, traversing the Cape Basin, can entrain and transport cold upwelled waters beyond the upwelling shelf (Duncombe Rae et al. 1992). However, there are also studies underscoring the role of cyclonic eddies in the upwelling system. Research by Giulivi and Gordon (2006), Souza et al. (2011), and Arhan et al. (2011) has demonstrated that orbital velocities within such eddies can reach 80 cm/s, and the core, characterized by strong temperature anomalies, is situated in the layer of 100–700 m. It is well-documented that upwelling eddies can significantly contribute to the offshore transport of substances (Ioannou et al. 2022, and references therein).

Mesoscale eddies, characterized by orbital velocities surpassing the speed of eddy propagation (Chelton et al. 2011; Gnevyshev et al. 2021), can retain water masses within their cores for prolonged periods during their propagation. Argo floats have provided crucial observations, with instances of being trapped by eddies in the Cape Basin and remaining within their cores for substantial durations (Malysheva et al. 2020; Guerra et al. 2022). Such eddies can serve as significant exporters of nutrients and biological components from coastal regions. The transport of upwelled waters into the sea influences biological productivity by redistributing phytoplankton and nutrients within or from the euphotic zone. Frontal zones can form on the periphery of vortices – areas with strong gradients of temperature, salinity, and water density, where different water masses interact (Fedorov 1986). These frontal zones typically host a large amount of plankton and concentrate nutrients (Mikaelyan et al. 2020, 2023; Kushnir et al. 2011; Russel et al. 1999).

It's important to note that in a mesoscale eddy of any polarity, there are regions where the thermocline is uplifted to the surface, creating conditions for increased chlorophyll-a concentration and enhanced bioproductivity (Mikaelyan et al. 2020). For example, a cyclonic eddy creates an uplift (dome-like bending) of isopycnals in both the thermocline and pycno-halocline, lifting the nitracline and promoting higher bioproductivity. In contrast, an anticyclonic eddy exhibits a sinking (depression) of the thermocline and pycno-halocline, negatively impacting bioproductivity. At the periphery of the eddy, there is an uplift of isopycnals, which, conversely, contributes to an increase in primary production. Unlike a typical anticyclone, a lens-shaped anticyclone induces upward water motion above the maximum velocity layer, often acting as a cyclone in its upper part (Mikaelyan et al. 2020).

In the study by Chernyshkov et al. (2005), five subregions were identified, differing like interannual variations in surface ocean thermal conditions. In the northern subregions, anomalies in sea surface temperature are formed under the influence of the equatorial heat

accumulation zone of the ocean. In the southern subregions, these anomalies are shaped by processes occurring in the eastern part of the subtropical gyre of the Southern Hemisphere. According to some data, the primary center of the Benguela upwelling is situated between 24°00'–26°25' and 27°00'–28°30'S (Shannon 1985; Stetsjuk 1983; Wysokinski 1986). The lowest mean water temperature throughout the year is observed in the Lüderitz region (26°30'S), while temperatures increase in the northern and southern directions (Lutjeharms and Meeuwis 1987). It should be noted that upwelling processes near Lüderitz exhibit a rapid response to changes in wind, lasting less than a day (Shannon 1985, 2001). Ship and satellite observations of surface water temperature from 1964 to 2002 indicate that the area occupied by waters cooler than 16°C extends along the entire coast (between 18° and 34°S) in winter (June–August) and spring (September–November) for a distance of up to 140 miles. In summer (December–February) and autumn (March–May), this area reduces in size, and apart from the zone of cold upwelling water within 20 miles from the coast, waters cooler than 16°C are only found between Wolfish Bay (23°S) and Cape Town (34°S). About 160 miles from the coast, the seasonal temperature variation in water is weak, indicating that the surface structures of the Benguela Current cover a zone about 160 miles wide (Babajan et al. 1985; Chernyshkov et al. 2005).

In contrast to the extensive studies conducted on northwest Africa upwelling (Sangrà et al. 2009), there is a notable scarcity of research focused on the transport of fluid elements by vortices in the Benguela upwelling area. Undoubtedly, the importance of studying vortices generated in the upwelling zone cannot be overstated, as quantitative assessments of their transport are essential for comprehending the dynamic processes in the water mixing zone that shape local marine ecosystems (Ioannou et al. 2022). Researchers have extensively studied vortices of non-upwelling origin in the Cape Basin and Agulhas Rings (see Malysheva et al. 2020; Gnevyshev et al. 2021; Sandalyuk and Belonenko 2021, and references therein). However, the vortices formed in the Benguela upwelling remain largely unexplored, despite their significant role in the region's dynamics.

The primary objective of this paper is to evaluate the impact of eddies originating from the Benguela upwelling on the region's dynamics. Specifically, we aim to address the following inquiries: (i) What are the characteristics of eddies formed directly within the Benguela upwelling zone? (ii) To what extent can these eddies transport the properties of upwelling-origin water parcels and influence the material transfer? (iii) How enduring are these eddies in retaining the properties of fluid? (iv) Does the alteration in the structure of these eddies influence their dynamics and, in particular, the nonlinearity parameter?

To explore these inquiries, we utilize Lagrangian modeling and the AMEDA approach, employing a diverse range of data sources.

2 Data and Methods

We use **the AVISO altimetry data** which are the result of combining measurements from all altimetry missions: Jason-3, Sentinel-3A, HY-2A, Saral/AltiKa, Cryosat-2, Jason-2, Jason-1, TOPEX/Poseidon, Envisat, GFO, ERS1/2. The Sea Level Anomalies (SLA) product for the period from 1993 to the present is available on the Copernicus Marine Environment Monitoring Service portal (CMEMS, http://marine.copernicus.eu/). The optimal interpolation method was used to combine the data. The spatial resolution of the interpolated array is 0.25° of latitude and longitude, and the temporal discreteness is 1 day (Le Traon et al. 2019). The latest array update includes a new sensor and atmospheric corrections, new calibration of various altimeters, new tide model and takes into account a longer base period of 20 years for estimating mean sea level (Pujol et al. 2016). The SLAs were calculated relative to the Mean Sea Surface (MSS) data available on the Aviso+ portal (Archiving, Validation, and Interpretation of Satellite Oceanographic Data, http://www.aviso.altimetry.fr/en/data/products/auxiliary-products/mss.html). We used the daily AVISO data from 1993 to 2020.

We also use the **Atlas of Altimetric Mesoscale Eddy Trajectories (META3.2 DT allsat).** It was prepared by SSALTO/DUACS and distributed by AVISO+ (https://www.aviso.altimetry.fr/) supported by CNES in collaboration with IMEDEA. The product is based on the use of altimetry information (sea surface heights) to identify and determine the trajectories of cyclones and anticyclones of the World Ocean (Pegliasco et al. 2022). The algorithm identifies isolated eddy structures on daily maps and then tracks them by recording their evolution over time. The algorithm identifies eddies as clusters of pixels (the maximum size is 2000 pixels) that satisfy a certain set of criteria, such as compactness, the presence of an extremum of sea level anomalies inside the eddy, etc. The Atlas assigns to each vortex its identification number and the coordinates of its trajectory. The META3.2 product contains information about the type of vortices, their radius and amplitude, orbital speed, and lifetime.

We use **GLORYS12V1 (Global Ocean Physics Reanalysis)** data available on the CMEMS (Copernicus Marine Environment Monitoring Service) portal. GLORYS12V1 is an eddy reanalysis of the World Ocean with a spatial resolution of 1/12° at 50 levels over the period when altimetry observations are available. It is based on the global real-time

forecasting system CMEMS. The NEMO (Nucleus for European Modelling of the Ocean, doi: 10.5281/zenodo.6334656 with ECMWF ERA-Interim forcing is used to simulate oceanic conditions. Observations are assimilated using a low-order Kalman filter. In situ, satellite altimeter data (sea level anomaly), sea surface temperature, sea ice concentration, and vertical profiles of temperature and salinity are assimilated together. This product includes daily 3D potential temperature, salinity, and current fields, as well as 2D level fields, depth of the upper quasi-homogeneous layer, potential bottom temperature, ice thickness, ice types, and ice drift velocities. The combined observations are Reynolds Sea surface temperature at 0.25° spatial resolution of the AVHRR sensor, level anomalies from all altimeters, temperature, and salinity profiles from the CMEMS CORAv4.1 database, and ice data from the CERSAT sea ice concentration database. The boundary conditions for temperature and salinity for 1991 are taken according to the EN.4.2.0 model. 1 and ice data from the CERSAT sea ice concentration database. The boundary conditions for the temperature and salinity for 1991 are taken according to EN4.0.2 (http://hadobs.metoffice.com/en4/download-en4-0-2.html). We analyze the GLORYS12V1 data at a depth of 21 m. We use the daily GLORYS12V1 data from 1993 to 2020.

The work also uses data from the global bathymetric-topographic model of the Earth's relief **ETOPO1** with a spatial resolution of 1' in latitude and longitude. The model combines data on the topography of the earth's surface and the bathymetry of the seabed. The bathymetric data in the ETOPO1 model are set by compiling data from the Japan Oceanographic Data Center (JODC), the Mediterranean Scientific Commission (Fr. Commission Internationale pour l'Exploration Scientifique de la Méditerranée – CIESM), the Caspian Environment Program (CEP) and the National Geophysical Data Center (NGDC).

We employ **Lagrangian methods** to analyze the transport and mixing of water particles within the study area. This approach involves computing the trajectories of a significant number of artificial passive particles. In turbulent or chaotic flows, plotting trajectories for an ensemble of particles, advected by either satellite-derived or numerical-model velocity fields, results in a complex network of intertwined lines that can be challenging to interpret. To address this complexity and enhance interpretation, we propose the use of specific trajectory functions known as Lagrangian indicators (Mendoza et al. 2010, 2014; Bettencourt et al. 2012; Beron-Vera et al. 2013; Prants et al. 2014, 2017; Lopesino et al. 2015; van Sebille et al. 2018; Budyansky et al. 2022). These indicators enable the extraction of valuable information about circulation from the intricate trajectories, offering a precise description of transport and mixing processes.

Lagrangian indicators are calculated by numerically advecting a dense mesh of numerous artificial particles.

In the Lagrangian approach, transport processes are monitored by tracking parcels of water represented by passive artificial particles. Various indicators can be constructed based on the research objectives. It is crucial to select a suitable time interval, taking into account the specificities of the oceanographic conditions in the study area. For this study, we opted for a duration of 365 days. It is worth noting that the calculations are conducted backward in time, commencing from a fixed date (Prants et al. 2014, 2017).

The Lagrangian indicator field is depicted on a basin Lagrangian map for each day. This sequence of maps enables the day-by-day tracking of the evolution of oceanographic parameter fields, facilitating the differentiation of water masses with distinct origins. Lagrangian fronts frequently align with confluence lines and vortex boundaries. Through the reverse-time analysis of simulation results, it becomes possible to ascertain the origin of fluid particles passing through a specific point. A considerable number of particles are dispersed across the study area, and the trajectories of Lagrangian particles are determined by solving the advection equations

$$\frac{d\lambda}{dt} = u(\lambda, \varphi, t), \frac{d\varphi}{dt} = v(\lambda, \varphi, t), \tag{1}$$

where u and v are angular zonal and meridional components of the AVISO velocity field, and φ and λ are latitude and longitude. Angular velocities are employed due to their maximally simple form on Earth's sphere. To ensure precision in numerical results, bicubic spatial interpolation and temporal evolution smoothing via third-order Lagrangian polynomials are implemented. The computation of Lagrangian trajectories involves integrating equations (1) using the fourth-order Runge-Kutta scheme with a constant time step of 0.001 days. Utilizing the Lagrangian analysis (please refer to Prants et al. 2017 for details), we scrutinize the Benguela upwelling and the eddies generated within the upwelling zone.

To identify vortex centers, daily positions of stationary points with zero velocity were computed. Subsequently, a standard stability analysis of linearized advection equations was performed to determine stable elliptic and hyperbolic points. Stable elliptic points (indicated by triangles on the maps) are generally located at the centers of vortices where rotation dominates over deformation. Hyperbolic points (crosses on the maps), where deformation dominates over rotation, are predominantly situated between vortices. Thus, the birth of a vortex is manifested by the appearance of a stable elliptic point, while its disappearance signals the vortex's decay. Hyperbolic points are also crucial because the stable and unstable manifolds associated with them organize flows around vortices, and facilitating water exchange between adjacent vortices (for more details, see please Prants et al. 2017).

To trace the history of water within vortices, Lagrangian Origin Maps (O-maps) were computed. By integrating transport equations backward in time, O-maps were generated, with particles colored according to the geographic boundary they crossed in the past. O-maps are parameterized by the initial day and an integration period empirically set at $T = 365$ days to track vortex water transport over a broad area for an extended duration. Lagrangian maps offer certain advantages compared to Eulerian characteristic maps, such as Sea Surface Height (SSH), vorticity, or the Okubo–Weiss parameter, which represent instantaneous snapshots of their respective fields. Lagrangian maps not only characterize the current state of a specific indicator field but also provide crucial information about the history and origin of water masses present in the study area. By sequentially examining daily Lagrangian maps, the evolution of chosen Lagrangian indicators' fields can be studied over an extended period (for more details, see Prants et al. 2017).

We used an optimized **algorithm AMEDA (Angular Momentum Eddy Detection and Tracking Algorithm)** for detecting and tracking eddies from two-dimensional velocity fields. This eddy identification uses a hybrid methodology based on physical parameters and is applied to the data of the reanalysis GLORYS12V1. For the detection and analysis of vortices, we chose the AMEDA algorithm (Le Vu et al. 2018). This hybrid method was selected for the following reasons:

- It is one of the most advanced eddy tracking algorithms, allowing not only the determination of vortex contours but also the calculation of many kinematic and dynamic characteristics.
- The vortex boundary is defined as the contour with the maximum mean rotational velocity around the center, which is found by maximizing the LNAM (Local and Normalized Angular Momentum) parameter. This approach avoids incorrect determination of vortex sizes (overestimating their area), unlike some methods that identify vortex boundaries based on SSH fields (e.g., META3.2).
- The algorithm incorporates a function for tracking events of vortex merging/separation, providing the opportunity for a more detailed analysis of inter-vortex water exchange situations occurring in the investigated region.

The main advantages of AMEDA are as follows: the algorithm is robust to the grid resolution, it uses a minimal number of tunable parameters, the dynamical features of the detected eddies are quantified, and the tracking procedure identifies the merging and splitting events (see pls Udalov et al. 2023). The proposed method provides a complete dynamical evolution of the detected eddies during their lifetime. This allows for identifying precisely the formation areas of long-lived eddies, the

region where eddy splitting or merging occurs frequently, and the interaction between eddies and oceanic currents. For each contour, the average orbital speed through circulation along the closed contour (flow) is determined by the average value of the radius, which is equivalent to the radius of a circle with the same area. The contour with the maximum orbital speed determines the size of the eddy (Le Vu et al. 2018).

Currently, several methods are used for the automatic detection of vortex structures in the World Ocean. Typically, satellite altimetry data, specifically the SSH field and the derived velocity field from AVISO, are employed. These methods enable the identification of daily positions of vortex centers and their contours. One widely used method is the algorithm proposed by Chelton et al. (2011), which is based solely on SSH field analysis. This algorithm found continuation and development in the META2.0 algorithm, which also relies on SSH field analysis. Faghmous et al. (2013) demonstrated that the threshold amplitude values used in the Chelton et al. (2011) method lead to incorrect estimates of vortex sizes (overestimating their area). A further development of the Chelton et al. (2011) method is found in the META3.2 algorithm based on the approach by Mason et al. (2014), which also utilizes the Sea Level Anomaly (SLA) and Absolute Dynamic Topography (ADT) fields. This improvement enhances the accuracy of vortex contour area determination and allows for the exclusion of contours with non-circular shapes. In the current version of META3.2, a new feature is added i.e. the construction of a vortex contour with the maximum vorticity value. This characteristic was proposed in AMEDA by Le Vu et al. (2018). A comparison of the results obtained using the META3.2 and AMEDA algorithms revealed that AMEDA identifies a greater number of vortices of both signs and enables tracking of vortex merging and splitting events. It is noteworthy that META3.2 contours have a polygonal shape because they are constructed based on 20 points, unlike AMEDA, where the number of points can vary from 20 to 100 (Pegliasco et al. 2022). However, the algorithm of AMEDA has a serious drawback since it is very difficult to use it for the region west of the prime meridian. This explains why we used both approaches (META3.2 and AMEDA).

So, the paper describes three possible ways to identify contours of eddies in datasets: a) reading them directly from the META3.2 dataset; b) using AMEDA on altimetric AVISO data; c) using AMEDA on reanalysis GLORYS12V1 data. Using these three data sets provides a comprehensive analysis of upwelling eddies in the Benguela region.

3 Results

3.1 Building an upwelling zone mask

We delineate an upwelling zone employing the GLORYS12V1 data spanning from 1993 to 2020, utilizing daily

surface data. In the initial phase, horizontal gradients in the temperature and salinity fields for each day are computed using the following formula:

$$|grad\ P| = \sqrt{\left(\frac{\partial P}{\partial x}\right)^2 + \left(\frac{\partial P}{\partial y}\right)^2} \tag{2}$$

Here, P denotes the parameter value (temperature or salinity), and ∂x and ∂y are the latitudinal and longitudinal steps, respectively, accounting for the geographical latitude of the location. The boundary of the upwelling zone is established as the boundary of the thermohaline front, with defined threshold values for the gradients. For temperature, a threshold value of $|grad\ T| \geq 0.02°$C km was used, and for salinity – $|grad\ S| \geq 0.01$ *psu*/km. The criteria selection is grounded on the outcomes of climatic averaging of hydrophysical fields, and optimal values are determined based on previous studies (Kostianoy et al. 2004; Ozhigin et al. 2016). Utilizing the daily GLORYS12V1 dataset spanning from 1993 to 2020, we computed the frequency of temperature and salinity gradient values surpassing predefined thresholds at each grid node. Subsequently, we identified nodes where the incidence of these values exceeded 50% individually for temperature and salinity during the period 1993–2020. Finally, we superimposed both regions, resulting in a mask of the upwelling zone, depicting concurrent threshold values for temperature and salinity. Figure 1a illustrates this mask as a shaded area. The approach of delineating the thermohaline front through the application of specific threshold values was validated in a study conducted by Travkin and Akhtyamova (2023). This method, considering the variability

of both temperature and salinity in the area, proves to be effective in accurately identifying the upwelling zone. This method is based on the calculation of the temperature and salinity on water surface gradients and allows us to determine the spatial location of the boundaries of the upwelling zone. We use the data inferred from the GLORYS12V1 dataset spanning from 1993 to 2020.
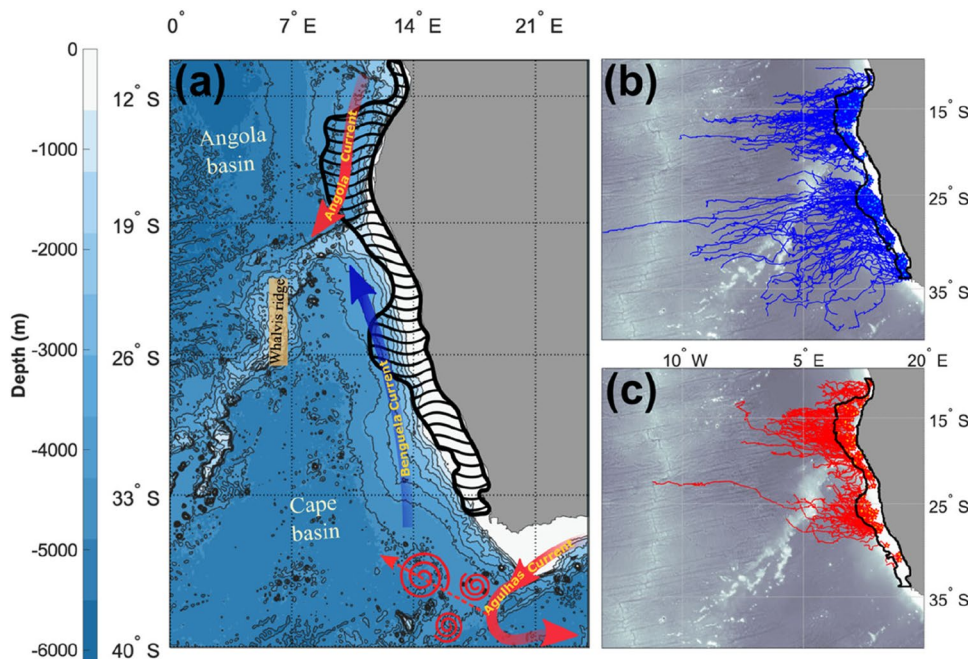
3.2 Eddies, generated in the upwelling zone

After the boundaries of the upwelling zone have become known, we apply the META3.2 data based on the AVISO dataset to consider the trajectories of eddies, the generation of which belongs to the upwelling zone. We use the META3.2 product because it is easy to interpret and very popular for analysis of eddy tracking. This product provides the trajectories of eddies extending far to the west. Figure 1(b and c) depicts the trajectories of cyclones and anticyclones originating within the Benguela upwelling zone (Fig. 1a) with a lifespan exceeding 2 months. Notably, both polarities of vortices are observed within the upwelling zone, but a visual examination of the track count suggests a significant predominance of cyclones. Detailed estimates in Table 1 further highlight that cyclones exhibit

Table 1 The number of cyclones and anticyclones with different lifespans (>2 months and >10 days) generated in the Benguela upwelling zone inferred from AVISO

	>2 months	>10 days
CEs	304	2157
AEs	230	1532

Fig. 1 The study area (**a**). The upwelling zone inferred from the GLORYS12V1 data averaged for 1993–2020 is shown by hatching. Tracks of cyclones (**b**) and anticyclones (**c**) formed in the upwelling zone inferred from META3.2 for 1993–2021 are shown

greater persistence than anticyclones, as evidenced by their longer trajectories. It is important to note that Table 1 includes only those Cyclonic Eddies (CEs) and Anticyclonic Eddies (AEs) generated in the Benguela upwelling zone.

Cyclones and anticyclones, influenced by the β-effect, exhibit westward movement, with anticyclones' trajectories showing a tendency to deflect toward the equator and cyclones' trajectories toward the South Pole. The β-effect's impact is extensively discussed in various papers, as analyzed by Gnevyshev et al. (2021). Additionally, visual analysis reveals an uneven generation of cyclones and anticyclones in the upwelling zone, suggesting the existence of

upwelling cells. Notably, the positioning of these cells for cyclones and anticyclones does not coincide.

The dominance of cyclones originating in the upwelling zone is further substantiated by Fig. 2. The illustration reveals that specific cells exhibit the formation of over 140 long-lasting cyclonic eddies (with a lifespan exceeding 10 days) during the designated timeframe. In contrast, the maximum count of long-lasting anticyclonic eddies formed within a cell is limited to 90.

Through Lagrangian backward-time analysis, we computed several Lagrangian indicators for each date spanning from 2010 to 2020 for AVISO and GLORYS12V1. As an illustrative example, Figure 3 portrays the Lagrangian

Fig. 2 The number of individual eddies, CE (**a**) and AE (**b**), calculated per one 1°×1° grid cell based on the META3.2 dataset for the period 1993–2021. The upwelling zone is indicated by the black line
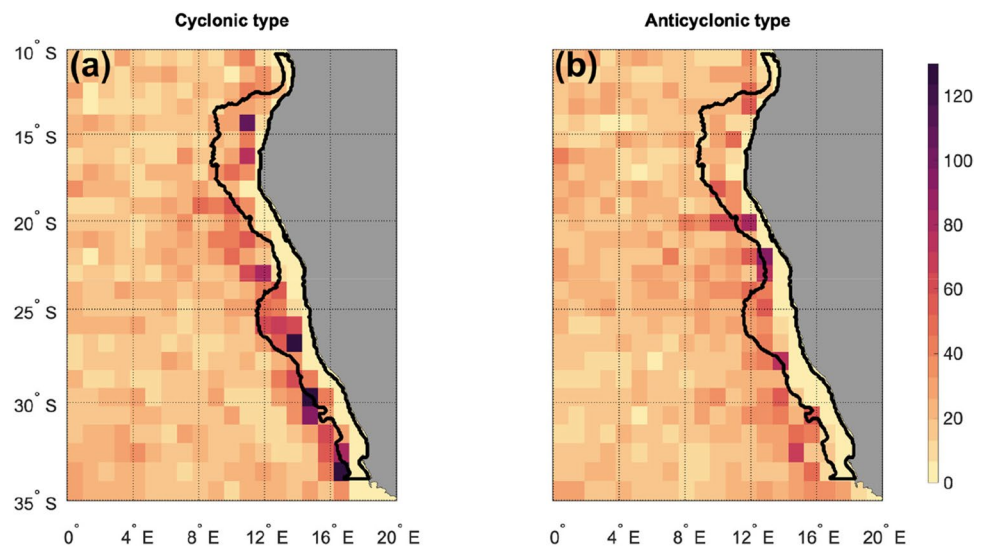
Fig. 3 The Lagrangian O- and T-maps in the area on 2011.03.01 are inferred from AVISO data. The O-map is on the left, and the T-map is on the right. The blue color points in the O-map correspond to the Lagrangian particles propagating from the upwelling area. The green and red colors in the T-maps correspond to the span of time (in days) and which the particles spent to reach these points from the upwelling area. The locations of eddy's centers are shown by ▼ for cyclones and ▲ anticyclones. The crosses show hyperbolic points that are points of instability (Prants et al. 2017)
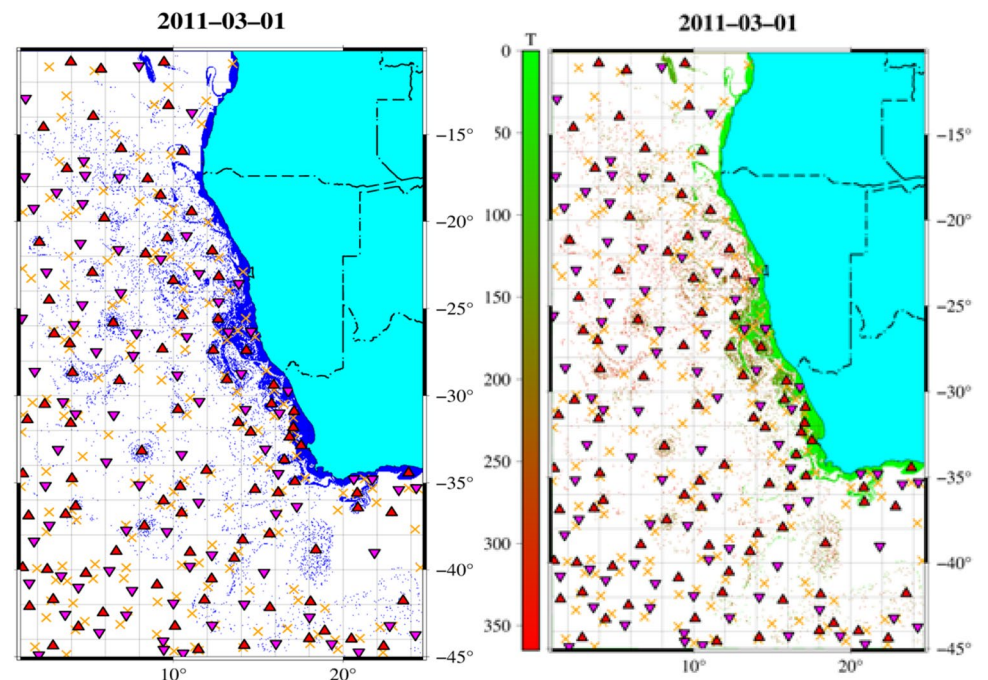
O- and T- maps in the region for a specific date (2011.03.01). A closer examination of Fig. 3 reveals further insights. The O-maps depict the spatial arrangement of Lagrangian particles, with their color indicating their source of origin. In particular, the blue color in the O-map delineates the distribution of Lagrangian particles originating from the Benguela upwelling zone, illustrating that fluid elements with upwelling origins are dispersed across almost the entire region. The Lagrangian particles depicted in blue exhibit filamentous patterns or cluster around the centers of eddies, as denoted by triangles. Notably, these particles travel significant distances from the Benguela upwelling zone, dispersing across the entire studied area. Given the varied propagation speeds of fluid elements from the upwelling zone, we have generated another map representing a Lagrangian indicator that delineates the propagation time of a particle from the upwelling zone to its current position. This is the T-origin map, which illustrates the propagation time of Lagrangian particles from the upwelling zone to their current positions, commonly referred to as "T-maps". In these maps, the green and red colors signify the time in days it took for each particle to travel to its present location. Green denotes points within or near the upwelling zone, with the time of spreading ranging from 0 to 365 days. Particles displaying red

coloration indicate those with properties akin to upwelling waters, positioned outside the upwelling zone, and correspond to particles with travel periods exceeding 200 days. The vortex centers were identified using Lagrangian methods as stable elliptic points where rotation dominates over deformation. The vortex centers are marked with triangles (Fig. 3). Figure 3 also reveals the prevalence of eddies in the coastal region, with cyclones being the dominant type among them.

The synthesis of Lagrangian modeling and AMEDA methods yielded the results presented in Fig. 4. The maps display the trajectories of long-lived eddy centers (lifetime > 10 days) based on AVISO altimetry data selected within the upwelling zone. For each day, the contour positions were determined using the AMEDA method, and the number of upwelling water parcels within each contour was identified. The proposed algorithm consists of the following steps (see also Udalov et al. 2023):

1. The study area (10°–45°S, 0°–25°E) was divided into a uniform grid of 600×600 nodes, and backward-time trajectories of Lagrangian particles were computed for each node for a period of one year from the date indicated on the map, covering each day from 2010 to 2020.
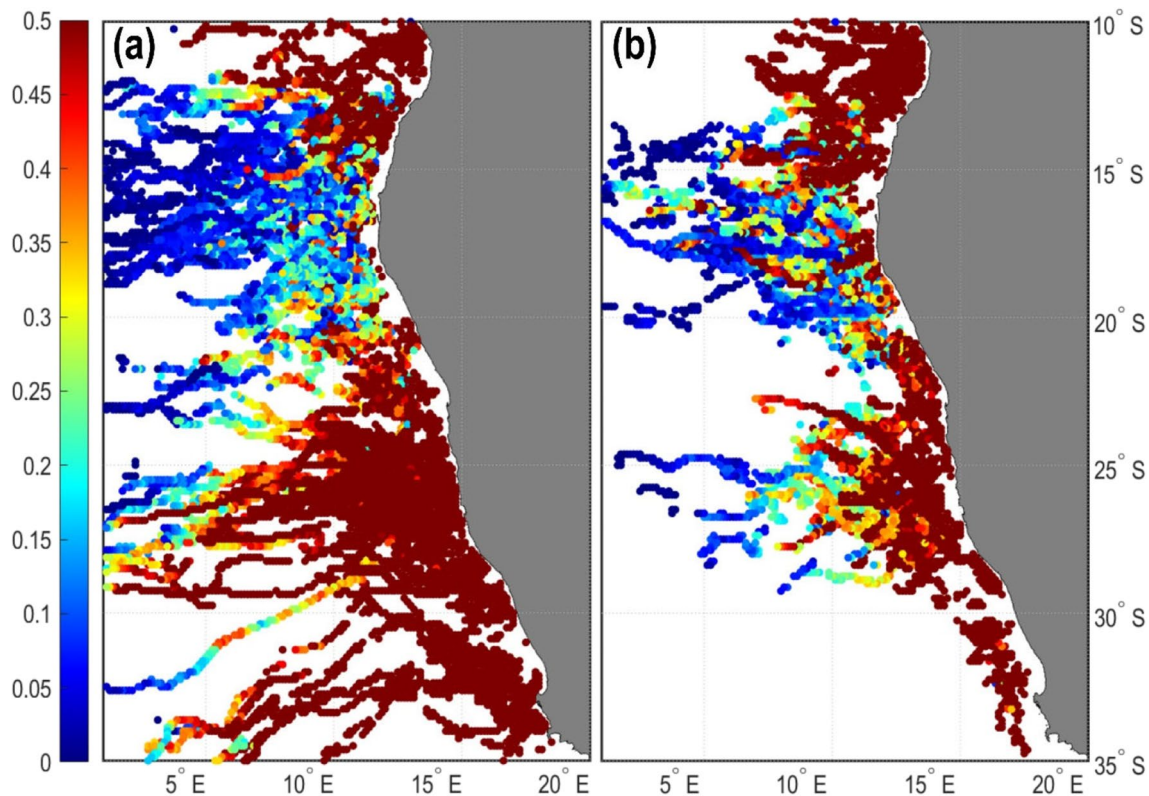

Fig. 4 The trajectories of CEs (**a**) and AEs (**b**), which were obtained using the AMEDA algorithm based on AVISO altimetry data. The color represents the current value of the markers' ratio, which simulates upwelling-origin waters, to the total number of artificial markers inside the eddy contour. A value of 0.5 indicates that half of the markers inside the eddy contour have an upwelling origin

2. As a result of step one, a set of origin maps (O-maps) was obtained. However, we are only interested in the grid nodes for which tracer trajectories touched the coast of Africa (the eastern boundary of the upwelling zone) and were located within the upwelling zone since these water parcels are regarded as upwelling waters.

3. Contours of detected eddies were placed on each O-map daily. So, the ratio of the number of nodes inside the contour where markers touched the coastline to the total number of grid nodes within the considered contour was calculated.

This approach allows for the calculation of the daily value of the ratio between the number of markers simulating upwelling-origin water parcels and the total number of markers within the eddy contour as the eddy moves. As a result, a color marker was assigned to each Lagrangian particle, with the color representing a specific value on the scale, reflecting the fraction of upwelling particles within the eddy contour at the given moment. As the eddy moves westward, the number of upwelling-origin particles within the eddy contours decreases. The value of 0.5 on the scale in Fig. 4 indicates that half of the markers within the contour have an upwelling origin.

From Fig. 4, it can also be observed that: (1) The number of CEs transporting westward captured waters within the contour significantly exceeds the number of AEs with upwelling waters. (2) The highest fraction of Lagrangian particles with upwelling-origin water properties is found within the vortex contours formed in the upwelling zone within the latitudinal bands of 10°–15°S and 20°–35°S. (3) Among the vortices formed in the upwelling zone, cyclones are more long-lived than anticyclones.

For subsequent analysis, only westward-traveling eddies that were initially filled with Lagrangian particles of upwelling origin at the time of eddy formation (plus the subsequent 5 days) were considered. Furthermore, we applied the empirical criterion for selecting vortices, which is based on the average ratio of the number of these particles to the total number of particles for the first 5 days of their existence, with a share of Lagrangian particles of upwelling origin >0.25. Given that the contour area, and hence the total number of Lagrangian particles, was determined by the AMEDA algorithm, the concentration of upwelling-origin elements within the vortices might vary.

One of the primary objectives of this study is to assess the residence time of upwelling-origin Lagrangian particles within the eddies and the distances traversed by these eddies. In this task, we only considered eddies for which the fraction of upwelling-origin artificial particles reached at least 0.5 at least once during the observation period, indicating that half of the particles within the contours of these vortices originated from upwelling.

Additionally, we calculated the transport time (in days) of eddies with Lagrangian particles of upwelling origin (Fig. 5a). We also determined the distance covered by the vortices during the observation period (Fig. 5b). As can be seen from Fig. 5, cyclones formed in the upwelling zone are much more persistent compared to anticyclones. Individual cyclones have a lifespan of approximately 500 days, while the lifespan of anticyclones doesn't exceed 300 days. This fundamentally distinguishes upwelling vortices from other mesoscale vortices in the Cape Basin with a different origin. For instance, studies (Malysheva et al. 2020; Gnevyshev et al. 2021) have shown that among eddies of Agulhas leakage, it is the anticyclones, not cyclones, that are long-lived and dominate in the region, covering the greatest distances as they move westward and even crossing the South Atlantic.

Figure 4 illustrates the gradual dissipation of fluid parcels of upwelling origin by eddies formed in the upwelling zone as they move westward. During their westward movement, vortices entrain filaments from the surrounding waters, incorporating them into their motion. This mixing with the surrounding waters results in the loss of particles

Fig. 5 The histogram shows the count of mesoscale upwelling-origin eddies based on their lifetime (days) and displacement (in kilometers) obtained using the AMEDA algorithm based on AVISO altimetry data for the period 2010–2020. The dark brown color indicates the overlap of blue and brown colors
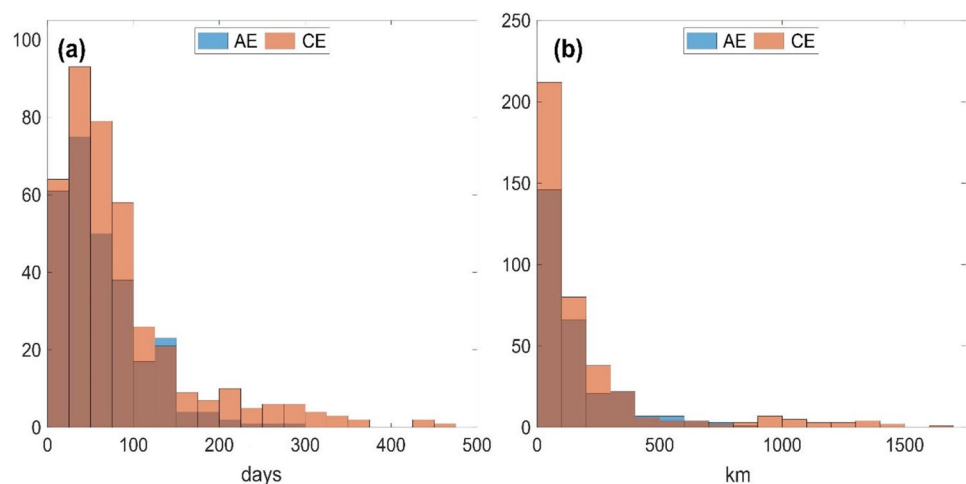
of upwelling origin by the vortices. In essence, the eddies experience water renewal and partial replacement of fluid parcels of upwelling origin with other water parcels (see pls Suppl. Mat.).

The upwelling zone exhibits lower values of temperature and salinity, as depicted in Figure 1a, which were previously utilized to delineate the maritime boundary of this region. However, as demonstrated earlier, upwelling waters actively engage with diverse dynamic structures, undergoing mixing with other waters. Figure 6a illustrates the westward extension of saline water tongues beyond the boundary of the upwelling zone. Nevertheless, as upwelling waters move westward, they also display meridional displacement both in the northern and southern directions. Figure 6b utilizes colors to represent the geographical latitude corresponding to fluid parcels of upwelling origin. Notably, the fluid parcels originating from a specific latitude of the upwelling zone can disperse considerably from their initial positions. Furthermore, it's essential to highlight that the localization

of fluid elements of upwelling origin in Fig. 6b frequently adopts a circular shape, indicative of vortex structures. The last is also evidenced by reduced salinity values in Fig. 6a in the vortices with upwelling origin.

To study the advection of fluid parcels of upwelling origin by eddies, we analyzed several tracks of eddies using the AMEDA and Lagrangian modeling using the GLORYS12V1 dataset. Figures 7 and 8 illustrate the progression of cyclones transporting westward fluid parcels with upwelling properties, while Fig. 9 displays the same for anticyclones. The tracks of cyclones are presented in Figs. 7a and 8a, with the fraction of Lagrangian particles of upwelling origin computed as the ratio of their number to the total number of artificial particles within each contour. The initial attribution of particles to upwelling-origin waters was determined using Lagrangian modeling (see Section 2). The color indicates the fraction of upwelling-origin waters within the contours. The vortices propagate westward under the influence of the β-effect,
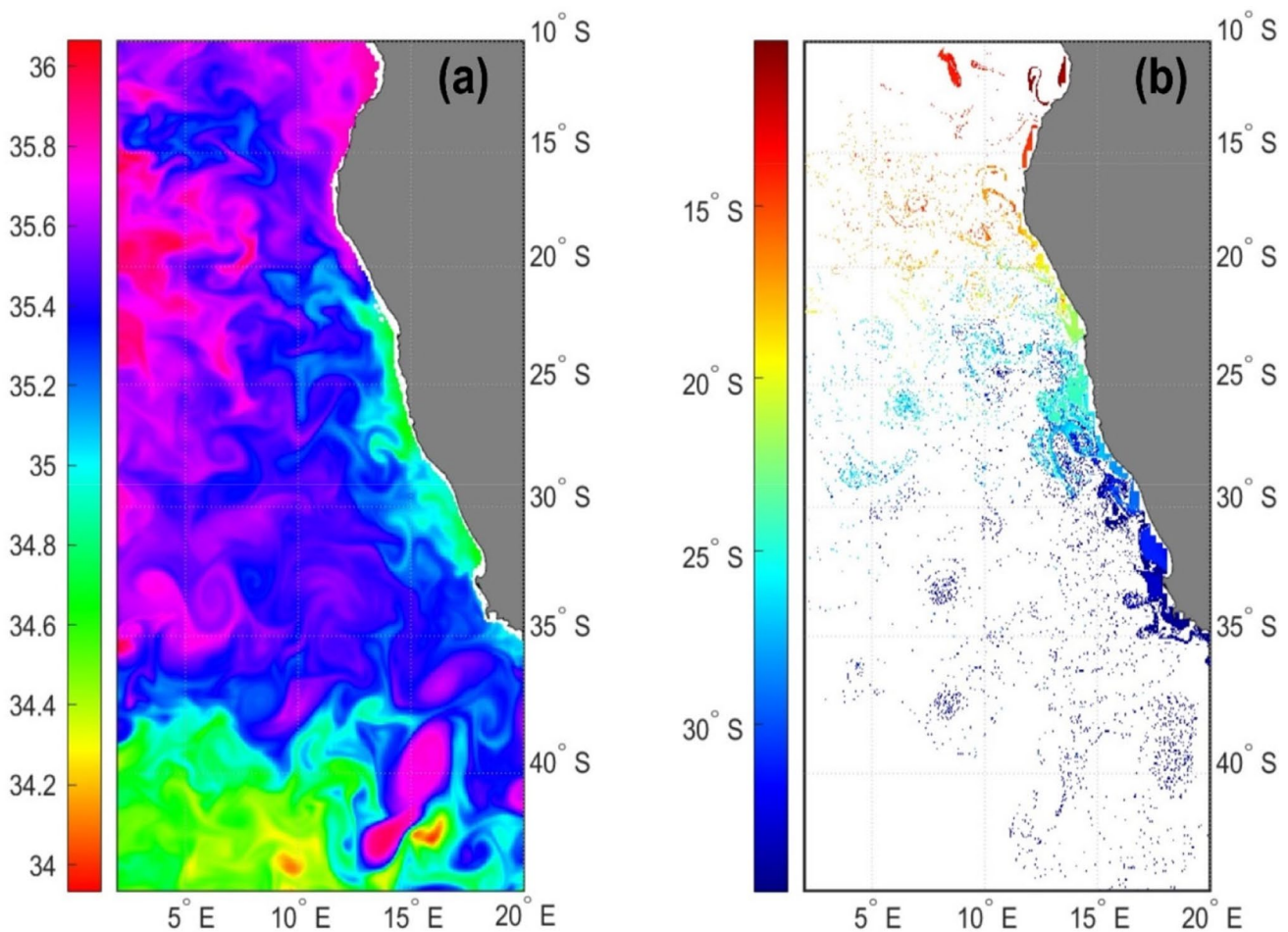

Fig. 6. (**a**) Spatial distribution of salinity in the study area at the depth of 21 m inferred from GLORYS12V1 data on 2011.03.01; (**b**) Map indicating the latitude where upwelling-origin particles were formed (Lagrangian φ-end-map) on 2011.03.01 inferred from GLORYS12V1 data, at the depth of 21 m. The color shows the value of latitude within 365 days from this date
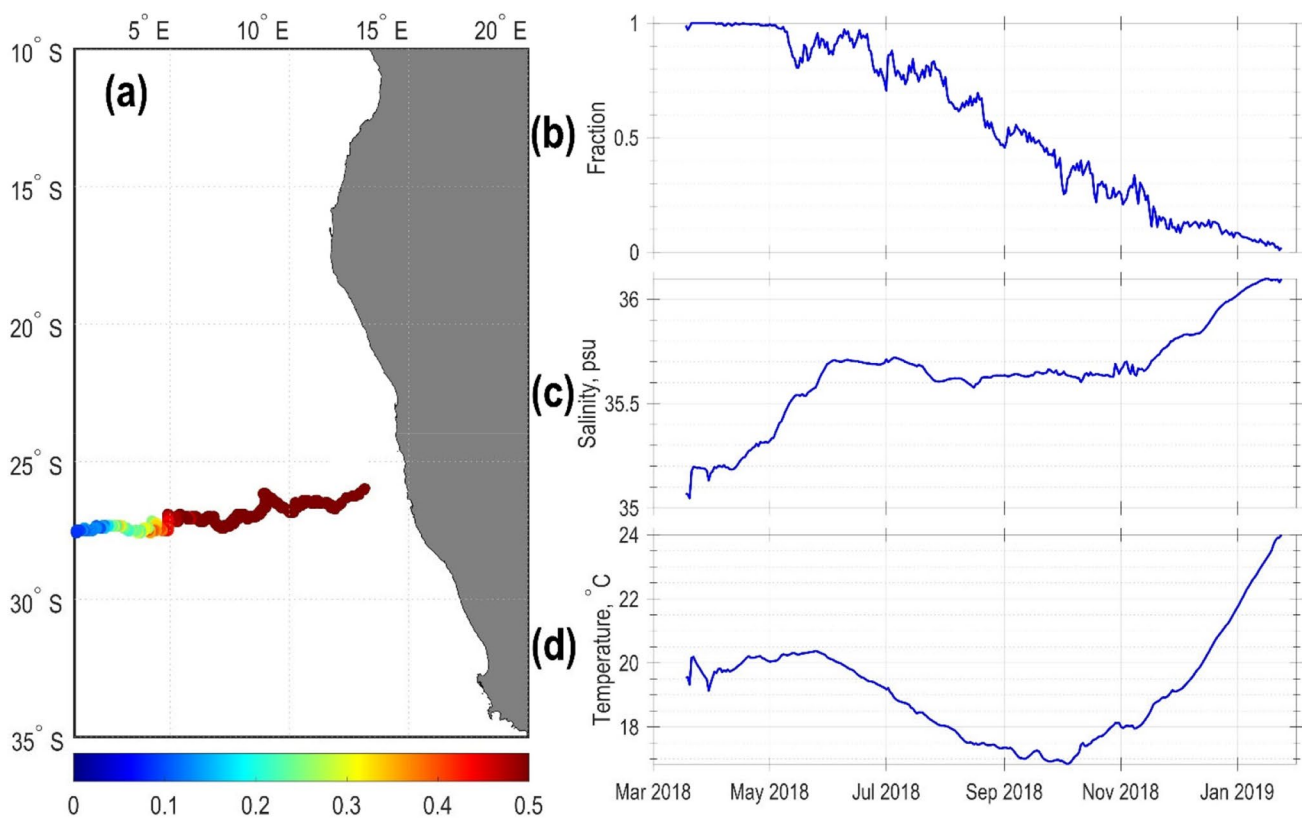
Fig. 7 The trajectory of cyclone #2215 using the AMEDA method based on GLORYS12V1 for the 21 m depth. The color bar corresponds to the fraction of upwelling-origin particles within the cyclone contours (**a**); temporal variability of the fraction of upwelling-origin particles within the cyclone contour (**b**); temporal variability of average salinity (**c**) and temperature (**d**) within the cyclone contour. The cyclone contours are overlaid on daily maps of temperature and salinity fields at the 21 m depth

and as they move, the fraction of Lagrangian particles of upwelling origin within the vortices gradually decreases. In the initial moment (March 2018), the fraction of upwelling-origin particles in the cyclone shown in Fig. 7a was 1 (100%), and this remained constant for two months. However, in May 2018, this fraction began to gradually decrease (Fig. 7b). By the end of January 2019, there were hardly any upwelling-origin particles left within the vortex contour. This example indicates that the vortex actively interacted with the surrounding waters, resulting in the gradual replacement of particles of upwelling origin within the vortex by other particles. This process was accompanied by an increase in salinity and temperature within the vortex (Fig. 7c, d). The proportion of fluid parcels of upwelling origin gradually decreased, and after a certain period, there were hardly any upwelling-origin particles left within the vortex contours. However, the cyclone continued its westward movement and dissipated only after 10 months. It is worth noting that despite the changes in the water structure, the vortex maintained its dynamics and continued to move westward.

Another example of a cyclone with a lifetime of 8 months is shown in Fig. 8. In contrast to the previous case, here the replacement of particles starts almost immediately, and after a month, only half of the particles within the vortex are particles of upwelling. Simultaneously, there are changes in salinity and temperature due to interactions with the surrounding waters, including the Agulhas leakage.

Figure 9a depicts the track of the anticyclone. It is evident that after leaving the upwelling zone, the anticyclone alters its course, initially moving northwest and then north. The lifespan of this anticyclone is approximately 4 months. In Fig. 9a and 9b, it is observed that after 2 months, the fraction of upwelling waters is halved, and by the conclusion of the anticyclone's life cycle, there are scarcely any upwelling-origin particles remaining within its contour. These particles within the anticyclone are supplanted by other particles drawn from the surrounding waters. The trajectory of the vortex in Fig. 9a illustrates the process of upwelling particle replacement within the vortex. Initially, the contour tracks were colored brown, indicating
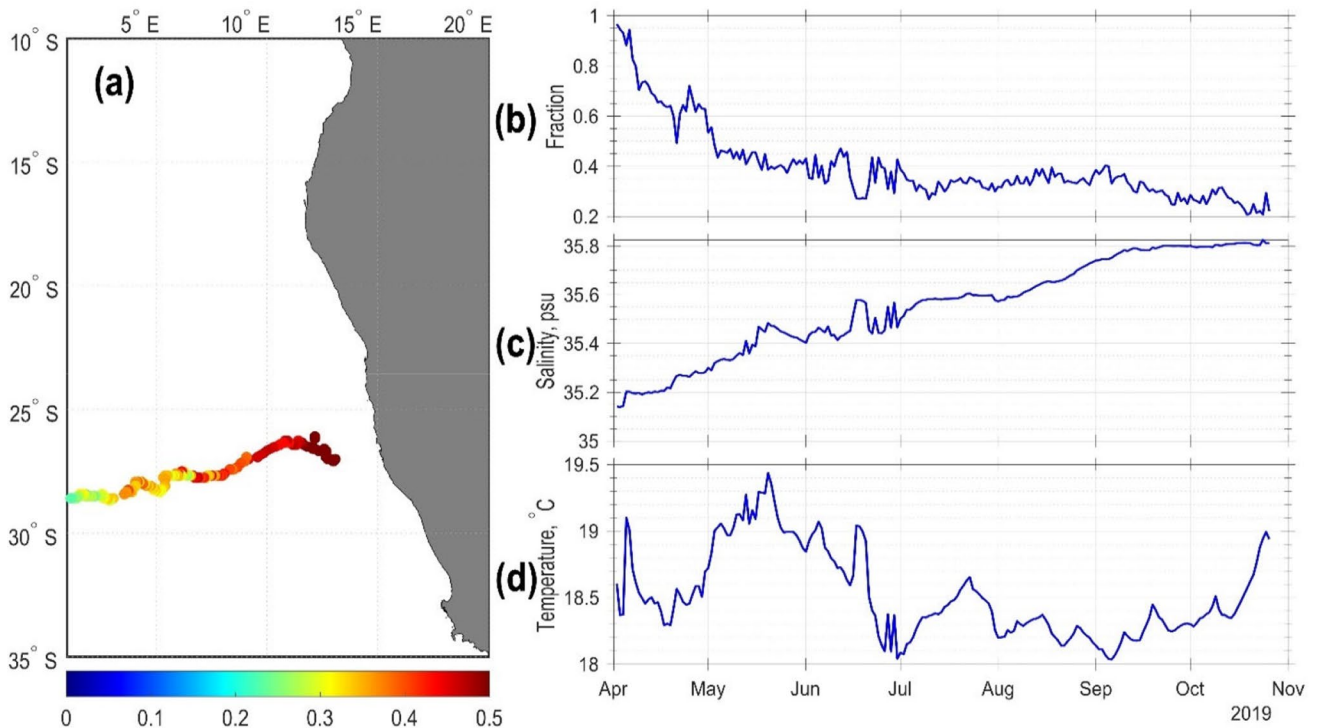
Fig. 8 The trajectory of cyclone 2412 using the AMEDA method based on GLORYS12V1 for the 21 m depth. The color bar corresponds to the fraction of upwelling-origin particles within the cyclone contours (**a**); temporal variability of the fraction of upwelling-origin particles within the cyclone contour (**b**); temporal variability of average salinity (**c**) and temperature (**d**) within the cyclone contour. The cyclone contours are overlaid on daily maps of temperature and salinity fields at the 21 m depth.

high values of the fraction of upwelling-origin particles, but later, the color shifts to blue. In the latter part of its life cycle, the vortex exhibits minimal movement, the contours overlap, and the fraction of upwelling-origin particles gradually diminishes from 0.5 to 0.1 and below. This process is accompanied by an increase in salinity and temperature within the vortex (Fig. 9c and d).

Additionally, we calculated the nonlinearity parameter for all the eddies under consideration. This parameter is defined as the ratio of the orbital velocity to the vortex translation speed. We observed the nonlinearity parameter behavior throughout the lifecycles of the eddies along their entire paths. Note, that although the nonlinearity parameter varied during the vortex's lifespan, it consistently remained above 1 for all the studied vortices. In the case of the three vortices analyzed, the nonlinearity parameter ranged from 2.5 to 3.5, consistent with estimates provided by Chelton et al. (2011) for this region.

4 Discussion and conclusions

The current understanding of how upwelling will evolve with climate change is characterized by uncertainty, but several projected changes align with existing climate models on both global and regional scales. In Bakun's hypothesis (1990), the increased emission of greenhouse gases in the future is anticipated to result in significant alterations in pressure gradients between land and sea. This, in turn, would impact global wind systems, potentially leading to heightened upwelling intensity across the World Ocean, particularly in the Benguela System. These projected changes encompass poleward shifts of dominant subtropical high-pressure systems, which play a crucial role in driving upwelling dynamics, ultimately leading to the intensification of upwelling in respective regions. Various climate change prediction models suggest the likelihood of prolonged seasons of intensified upwelling in the Benguela System in the future (Bograd et al. 2023). Collectively, these findings imply that the influence of the Benguela upwelling system on the region is poised to continue growing.

Several Lagrangian methods for eddy identification in the Benguela upwelling area have been developed by various authors, including Rossi et al. (2008, 2009) and Dräger-Dietel et al. (2018). In our investigation, we employed a combination of Lagrangian modeling developed by Prants et al. (2014, 2017) and the AMEDA (Agulhas and Madagascar Eddy Dynamics and Mixing) method, utilizing data from the GLORYS12V1 global ocean reanalysis, altimetry data, and the Mesoscale Eddy Trajectories Atlas product (META3.2
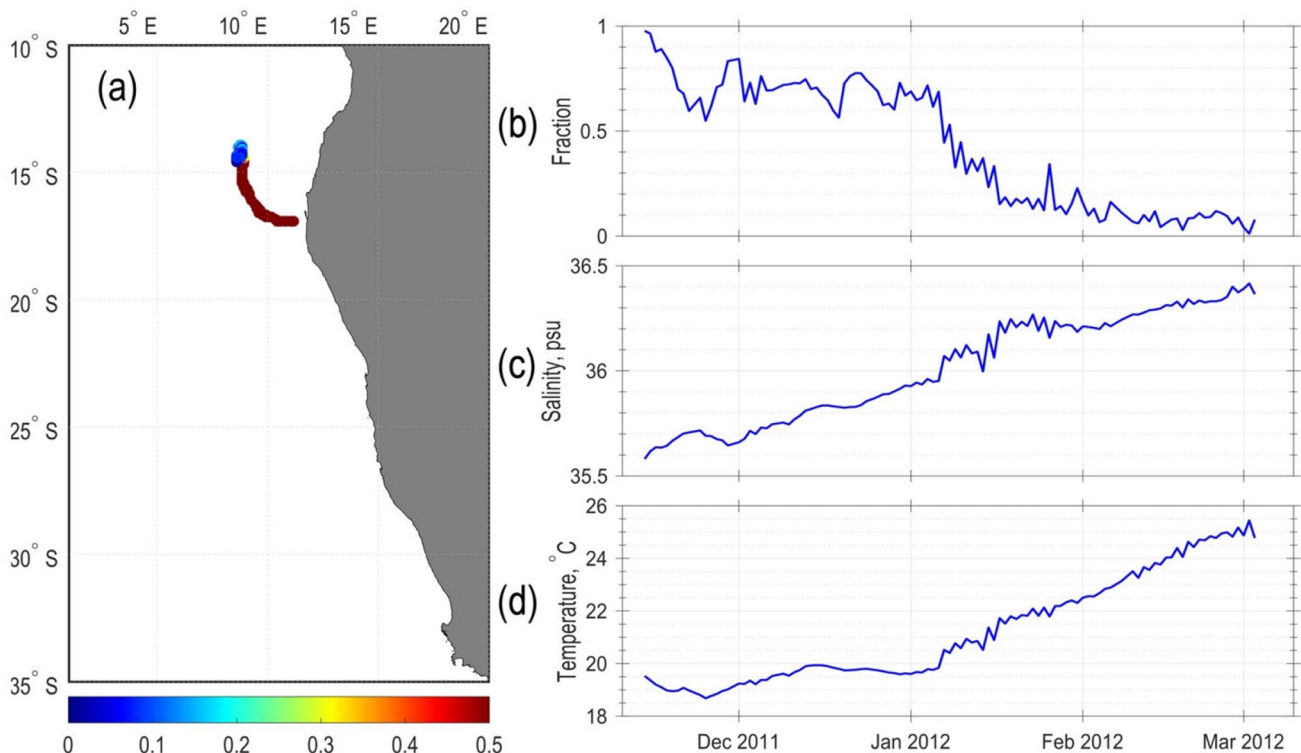
Fig. 9 The trajectory of anticyclone 1019 using the AMEDA method based on GLORYS12V1 for the 21 m depth. The color bar corresponds to the fraction of upwelling-origin particles within the anticyclone contours (**a**); temporal variability of the fraction of upwelling-origin particles within the cyclone contour (**b**); temporal variability of average salinity (**c**) and temperature (**d**) within the anticyclone contour. The anticyclone contours are overlaid on daily maps of temperature and salinity fields at the 21 m depth

DT). The integration of AMEDA contours with Lagrangian and Eulerian characteristics, calculated from reanalysis data, facilitates a direct comparison of thermodynamic and Lagrangian properties of waters and eddies. This approach offers an efficient means of obtaining relevant research information with reduced computational costs. The application of this methodological arsenal to the utilized datasets has yielded a set of conclusions that underscore the novelty of our study. Specifically, we focused on the 21 m layer to delineate the seaward boundary of the upwelling zone.

Our findings highlight the prevalence of upwelling cyclones in the studied region. Notably, cyclones originating within the upwelling zone exhibit greater stability and longer lifespans compared to their anticyclonic counterparts. Under the influence of the β-effect, cyclones cover more extensive distances during westward movement, with a range of 500 km compared to the 300 km traveled by anticyclones. This distinction underscores a fundamental difference between vortices of upwelling origin and other mesoscale vortices in the region, where anticyclones typically dominate across various properties (see references in Malysheva et al. 2020; Gnevyshev et al. 2021). Several studies have emphasized the significance of cyclonic vortices formed within the upwelling zone (Giulivi and Gordon

2006; Souza et al. 2011; Arhan et al. 2011). Nevertheless, the role of anticyclonic vortices in transporting waters of upwelling origin has remained unclear. In our investigation, we illustrate that anticyclones are indeed generated within the Benguela upwelling zone. Although the number of anticyclones is notably lower than cyclones, and their trajectories are shorter, anticyclones originating from upwelling also contribute to the region's dynamics and play a role in water mixing. Thus, we have established the influence of Benguela upwelling anticyclones on the region.

The Benguela upwelling region is renowned for hosting distinct upwelling cells, a characteristic linked to the seabed's topographic features and the coastline's shape (Shannon 1985, 2001; Lutjeharms and Meeuwis 1987; Chernyshkov et al. 2005). The upwelling intensity induces various instabilities along the coastline, giving rise to the creation of mesoscale eddies. In our analysis, we obtained the spatial distribution of cells indicating the number of eddies generated in each cell. These are climatological values of both cyclonic and anticyclonic eddies, encompassing eddies in the Benguela upwelling zone. Notably, the geographical distribution of maximum generation values for cyclones and anticyclones differs suggesting that cyclones predominantly form in certain cells, while anticyclones form in others.

The distribution of upwelling waters in the region is evident in spatial patterns showcasing reduced salinity values. The upwelling zone is distinctly recognizable on maps depicting the spatial distribution of salinity. This empirical method is frequently utilized by researchers to ascertain the upwelling zone boundaries (see the review in Ioannou et al. 2022). In contrast to this conventional approach, our study takes into account both salinity and water temperature. The overlay of maps illustrating salinity and temperature gradients enabled precise delineation of the geographical extent of the upwelling zone (see Section 3.1).

Utilizing Lagrangian modeling and AMEDA methods, we illustrated the observed westward advection of particles originating from the Benguela upwelling. Our results indicate that these particles exhibit not only zonal movement but also meridional transport, effectively filling the entire selected study region.

We have demonstrated that eddies induced by upwelling effectively entrain and transport water westward. In this study, we introduced a novel approach that combines kinematic information from AMEDA (providing the position and contour area of selected vortices) with Lagrangian modeling (providing maps of the origin and distribution of temperature and salinity). By integrating Lagrangian modeling and AMEDA methods, we constructed contours of mesoscale upwelling-origin eddies with lifespans exceeding 1 day and analyzed the origin of fluid elements within these contours. This analysis allowed us to estimate the fraction of upwelling-origin particles captured within the eddy relative to the total number of artificial particles within the contour. Our findings indicate that eddies with lifespans of several months only

transport upwelling-origin particles for a small portion of this time, primarily during their generation in the upwelling zone. As these eddies move westward, they gradually lose upwelling-origin particles, which are subsequently replaced by other fluid elements entrained from the surrounding waters. The animation (see Suppl. Mat., please) illustrates the change in the position of the vortex (cyclone) contours. The red color indicates the cluster of markers simulating upwelling-origin particles. By the midpoint of the eddy's path, the fraction of upwelling-origin particles within it can decrease by 2–4 times. Nevertheless, these eddies retain their dynamic structure characterized by dominant rotational motions.

Figures 7, 8, and 9 display three examples (two cyclones and one anticyclone), demonstrating a consistent reduction in the concentration of particles originating from upwelling within the contours of the vortices. After considering three examples of eddies using the GLORYS12V1 data set (Figs. 7, 8 and 9) we obtained in the next step the generalized graphs for all CEs and AEs in the study area demonstrating the temporal variability of upwelling-origin particle's fraction within the eddies. Figure 10 summarizes the result for all eddies using the GLORYS12V1 data set. This shows that CEs and AEs lose gradually particles of upwelling origin which are replaced by other particles coming into the contours from the outside.

The key inference from this analysis is that these eddies undergo structural and property changes as they progress westward. Both cyclones and anticyclones experience a gradual loss of fluid particles, subsequently replaced. This phenomenon is illustrated through specific examples. The timeframe during which it can be asserted that the eddy
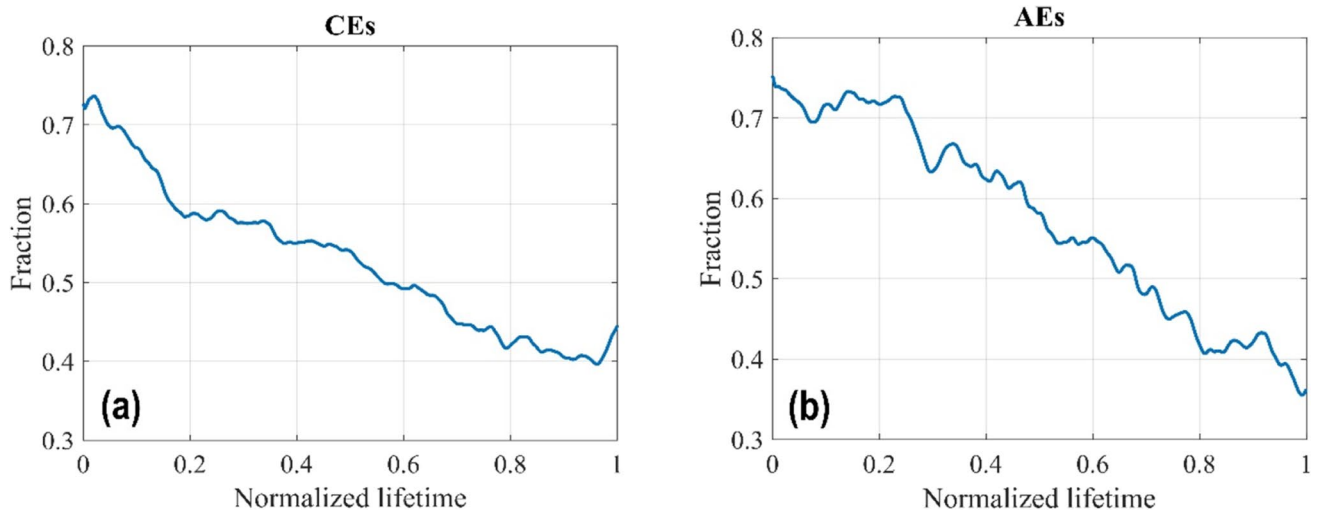

Fig. 10 Generalized time courses in the proportion of particles originating from upwelling within the contours of Cyclonic Eddies (CEs) (**a**) and Anticyclonic Eddies (AEs) (**b**) according to the GLORYS-12V1dataset for the 21 m depth. The *x*-axis depicts the normalized lifetime of vortices, while the *y*-axis shows the fraction of the particles in the contours

transports Lagrangian particles of upwelling origin, captured through rotation during its westward motion, constitutes only a portion of its lifecycle. However, it is crucial to highlight that, at the same time, the eddy maintains its dynamic properties consistently throughout its existence and has a nonlinearity parameter greater than one. This implies that the nonlinearity parameter, traditionally used to characterize the capture and transport of rotating fluid elements over long distances, may not provide an unambiguous representation, as previously assumed (Flierl 1981; Chelton et al. 2011; Morrow and Le Traon 2012). Our specific examples illustrate that, by the end of their trajectory, eddies transport entirely new water parcels. Therefore, our results emphasize that an orbital velocity surpassing the translation velocity of the eddy and nonlinearity parameters >1 do not necessarily indicate the long-distance transport of fluid parcels initially captured by rotation. We have demonstrated that eddies lose the fluid elements initially captured by rotation, gradually replacing them with other water parcels entrained from the surrounding waters. This finding holds significant implications.

Nevertheless, it is crucial to recognize that this approach comes with inherent limitations concerning the representation of 3D hydrological fields within a 2D framework. These limitations arise from the application of 2D Lagrangian analysis to a three-dimensional ocean. Our calculations of particle trajectories and concentration within eddies span one-year periods at a depth of 21 meters (refer to Figs. 4, 6, and 7). We have validated our findings through cross-referencing with AVISO data. Leveraging our previous experience in Lagrangian modeling using AVISO and reanalysis data (see Budyansky et al. 2022; Prants et al. 2014, 2017, 2018; Udalov et al. 2023 and references therein), we can confidently assert that this approach facilitates the tracking of particle transport pathways, including the most probable routes of Lagrangian particles by eddies, despite the inherent constraints of the 2D representation.

Declarations

References

Arhan M, Speich S, Messager C et al (2011) Anticyclonic and Cyclonic Eddies of Subtropical Origin in the Subantarctic Zone South of Africa. J Geophys Res: Oceans 116:1–22. https://doi.org/10.1029/2011JC007140

Babajan V, Kolarov P, Prodanov K, Vaske B, Wysokinski A (1985) Stock assessment and catch projections for Cape horse mackerel in ICSEAF Divisions 1.3+1.4+1.5. Colln Scient Pap Int Commn SE Atl Fish 12:39–48

Bakun A (1990) Global climate change and intensification of coastal ocean upwelling. Science 247:198–201

Beron-Vera FJ, Wang Y, Olascoaga MJ, Goni GJ, Haller G (2013) Objective Detection of Oceanic Eddies and the Agulhas Leakage. J Phys Oceanograp 43(7):1426–1438. https://doi.org/10.1175/JPO-D-12-0171.1

Bettencourt JH, López C, Hernández-García E (2012) Oceanic three-dimensional Lagrangian coherent structures: A study of a mesoscale eddy in the Benguela upwelling region 51:73–83. https://doi.org/10.1016/j.ocemod.2012.04.004

Bograd SJ, Jacox MG, Hazen EL, Lovecchio E, Montes I, Pozo Buil M, Shannon LJ, Sydeman WJ, Rykaczewski RR (2023) Climate Change Impacts on Eastern Boundary Upwelling Systems. Ann Rev Mar Sci 15:303–328. https://doi.org/10.1146/annurev-marine-032122-021945

Budyansky MV, Prants SV, Uleysky MY (2022) Odyssey of Aleutian eddies. Ocean Dyn 72:455–476. https://doi.org/10.1007/s10236-022-01508-w

Chelton DB, Schlax MG, Samelson RM (2011) Global Observations of Nonlinear Mesoscale Eddies. Prog Oceanography 91:167–216. https://doi.org/10.1016/j.pocean.2011.01.002

Chernyshkov PP, Sirota AM, Timokhin EV (2005) Structure and dynamics of waters in the areas of the Canary and Bengal upwelling and their influence on pelagic fish populations. Atlant-NIRO, Kaliningrad (in Russian)

Dräger-Dietel J, Jochumsen K, Griesel A, Badin G (2018) Relative dispersion of surface drifters in the Benguela upwelling region. J Phys Oceanogra 48(10):2325–2341. https://doi.org/10.1175/JPO-D-18-0027.1

Duncombe Rae C, Shillington F, Agenbag J, Taunton-Clark J, Gründlingh M (1992) An Agulhas Ring in the South Atlantic Ocean and its Interaction With the Benguela Upwelling Frontal System. Deep Sea Research Part A. Oceanogr Res Papers 39:2009–2027. https://doi.org/10.1016/0198-0149(92)90011-H

Faghmous JH, Le M, Uluyol M, Kumar V., and Chatterjee SB (2013) A parameter-free spatio-temporal pattern mining model to catalog

global ocean dynamics, in: Proceedings – IEEE International Conference on Data Mining, ICDM, 13th IEEE International Conference on Data Mining, ICDM 2013, 151–160, https://doi.org/10.1109/ICDM.2013.162, 2013

Fedorov KN (1986) The Physical Nature and Structure of Oceanic Fronts. Springer-Verlag, Berlin

Fedorov AM, Belonenko TV, Budyansky MV, Prants SV, Uleysky MY, Bashmachnikov IL (2021) Lagrangian Modelling of Water Circulation in the Lofoten Basin. Dyna Atmospheres Oceans 96:101258. https://doi.org/10.1016/j.dynatmoce.2021.101258

Fennel W, Seifert T (1995) Kelvin wave controlled upwelling in the western Baltic. J Marine Systems 6:289–300

Flierl GGR (1981) Particle motions in large-amplitude wave fields. Geophys Astrophys Fluid Dyn 18(1–2):39–74. https://doi.org/10.1080/03091928108208773

Giulivi CF, Gordon AL (2006) Isopycnal Displacements Within the Cape Basin Thermocline as Revealed by the Hydrographic Data Archive. Deep Sea Res Part I: Oceanogr Res Papers 53:1285–1300. https://doi.org/10.1016/j.dsr.2006.05.011

Gnevyshev VG, Malysheva AA, Belonenko TV, Koldunov AV (2021) On Agulhas Eddies and Rossby Waves Travelling by Forcing Effects. Russian Journal of Earth Sciences 21(5): ES6003, https://doi.org/10.2205/2021ES000773

Ioannou A, Speich S, Laxenaire R (2022) Characterizing Mesoscale Eddies of Eastern Upwelling Origins in the Atlantic Ocean and Their Role in Offshore Transport. Front Mar Sci 9:835260. https://doi.org/10.3389/fmars.2022.835260

Kahru M, Håkansson B, Rud O (1995) Distributions of the sea-surface temperature fronts in the Baltic Sea as derived from satellite imagery. Cont Shelf Research 15(6):663–679

Kostianoy AG, Nihoul JCJ, Rodionov VB (2004), Physical Oceanography of Frontal Zones in the Subarctic Seas. Elsevier Oceanography Series

Kushnir V, Pavlov V, Morozov A, Pavlova O (2011) "Flashes" of chlorophyll-a concentration derived from in situ and remote sensing data at the Polar Front in the Barents Sea. Open Oceanograp J 5:14–21. https://doi.org/10.2174/1874252101105010014

Le Traon PY, Reppucci A, Alvarez Fanjul E et al (2019) From observation to information and users: The Copernicus Marine Service perspective. Front Mar Sci 6:234. https://doi.org/10.3389/fmars.2019.00234

Le Vu B, Stegner A, Arsouze T (2018) Angular Momentum Eddy Detection and Tracking Algorithm (AMEDA) and Its Application to Coastal Eddy Formation. J Atmospheric Oceanic Technol 35(4):739–762. https://doi.org/10.1175/JTECH-D-17-0010.1

Lopesino C, Balibrea-Iniesta F, Wiggins S, Mancho AM (2015) The Chaotic Saddle in the Lozi Map, Autonomous and Nonautonomous Versions. Int J Bifurcation Chaos 25(13):1550184. https://doi.org/10.1142/S0218127415501849

Lutjeharms JRE, Meeuwis JM (1987) The extent and variability of South-East Atlantic upwelling. South African J Marine Sci 5(1):51–62. https://doi.org/10.2989/025776187784522621

Malysheva AA, Kubryakov AA, Koldunov AV, Belonenko TV (2020) Estimating Agulhas Leakage by Means of Satellite Altimetry and Argo Data. Izvestiya, Atmospheric Oceanic Phys 56:1581–1589. https://doi.org/10.1134/S0001433820120476

Manta G, Speich S., Karstensen J, Hummels R, Kersalé M., Laxenaire R, et al. (2021). The South Atlantic Meridional Overturning Circulation and Mesoscale Eddies in the First GO-SHIP Section at 34.5°S. J. Geophys. Res.: Oceans 126, e2020JC016962. https://doi.org/10.1029/2020JC016962

Mason E, Pascual A, McWilliams JC (2014) A New Sea Surface Height-Based Code for Oceanic Mesoscale Eddy Tracking. J Atmos Ocean Tech 31:1181–1188. https://doi.org/10.1175/JTECH-D-14-00019.1

Mendoza C, Mancho AM, Rio M-H (2010) The turnstile mechanism across the Kuroshio current: analysis of dynamics in altimeter velocity fields. Nonlinear Proc Geophys 17(2):103–111. https://doi.org/10.5194/npg-17-103-2010

Mendoza C, Mancho AM, Wiggins S (2014) Lagrangian descriptors and the assessment of the predictive capacity of oceanic data sets. Nonlinear Proc Geophys 21(3):677–689. https://doi.org/10.5194/npg-21-677-2014

Mikaelyan AS, Zatsepin AG, Kubryakov AA, Podymov OI, Mosharov SA, Pautova LA, Fedorov AV, Ocherednik OA (2023) Case where a mesoscale cyclonic eddy suppresses primary production: A Stratification-Lock hypothesis. Prog Oceanograp 212:102984. https://doi.org/10.1016/j.pocean.2023.102984

Mikaelyan AS, Zatsepin AG, Kubryakov AA (2020) Effect of Mesoscale Eddy Dynamics on Bioproductivity of the Marine Ecosystems (Review). Physical Oceanography [e-journal] 27(6):590–618. https://doi.org/10.22449/1573-160X-2020-6-590-618

Moroshkin KV, Bubnov VA, Bulatov RP (1970) Water circulation in the eastern South Atlantic Ocean. Oceanology 10:27–34

Morrow R, Le Traon PY (2012) Recent advances in observing mesoscale ocean dynamics with satellite altimetry. Adv Space Res 50(8):1062–1076. https://doi.org/10.1016/j.asr.2011.09.033

Neiman G (1973) Ocean currents. Hydrometeoizdat, Leningrad (in Russian)

Ozhigin VK, Ivshin VA, Trofimov AG et al (2016) The Barents Sea water: structure, circulation, variability. PINRO, Murmansk (in Russian)

Pavlushin VA, Kubryakov AA (2022) Seasonal and Interannual Variability of the Thermohaline Structure of the Bengel Upwelling Based on the Argo Buoys Data. Physical Oceanography [e-journal] 29(1):15–29

Pegliasco C, Chaigneau A, Morrow R (2015) Main Eddy Vertical Structures Observed in the Four Major Eastern Boundary Upwelling Systems. J Geophys Res: Oceans 120:6008–6033. https://doi.org/10.1002/2015JC010950

Pegliasco C, Delepoulle A, Mason E, Morrow R, Faugère Y, Dibarboure G (2022) META3.1exp: a new global mesoscale eddy trajectory atlas derived from altimetry. Earth Syst Sci Data 14:1087–1107. https://doi.org/10.5194/essd-14-1087-2022

Prants SV, Budyansky MV, Uleysky MY (2014) Identifying Lagrangian fronts with favourable fishery conditions. Deep Sea Research Part I: Oceanograp Res Papers 90:27–35. https://doi.org/10.1016/j.dsr.2014.04.012

Prants SV, Uleysky MY, Budyansky MV (2017) Lagrangian Oceanography: Large-scale Transport and Mixing in the Ocean. Springer-Verlag

Prants SV, Budyansky MV, Uleysky MY (2018) How eddies gain, retain, and release water: a case study of a Hokkaido anticyclone. Geophys Res Lett 123(3):2081–2096. https://doi.org/10.1002/2017jc013610

Pujol M-I, Faugère Y, Taburet G, Dupuy S, Pelloquin C, Ablain M, Picot N (2016) DUACS DT2014: the new multi-mission altimeter data set reprocessed over 20 years. Ocean Sci 12(5):1067–1090. https://doi.org/10.5194/os-12-1067-2016

Rossi V, López C, Sudre J, Hernández-García E, Garçon V (2008) Comparative study of mixing and biological activity of the Benguela and Canary upwelling systems. Geophys Res Lett 35(11):L11602. https://doi.org/10.1029/2008gl033610

Rossi V, López C, Hernández-García E, Sudre J, Garçon V, Morel Y (2009) Surface mixing and biological activity in the four Eastern Boundary Upwelling Systems Nonlin. Proc Geophys 16:557–568. https://doi.org/10.5194/npg-16-557-2009

Russell RW, Harrison NM, Hunt JGL (1999) Foraging at a Front: Hydrography, Zooplankton, and Avian Planktivory in the Northern Bering Sea. Mar Ecol Prog 182:77–93. https://doi.org/10.3354/meps182077

Sandalyuk NV, Belonenko TV (2021) Three-Dimensional Structure of the mesoscale eddies in the Agulhas Current region from hydrological and altimetry data. Russ J Earth Sci 21:ES4005. https://doi.org/10.2205/2021ES000764

Sangrà P, Pascual A, Rodríguez-Santana Á, Machín F, Mason E, McWilliams JC et al (2009) The Canary Eddy Corridor: A Major Pathway for Long-Lived Eddies in the Subtropical North Atlantic. Deep Sea Res Part I: Oceanogr Res Papers 56:2100–2114https://doi.org/10.1016/j.dsr.2009.08.008

Shannon LV (1985) The Benguela ecosystem I. Evolution of the Benguela, physical features and processes. Oceanograp Marine Bio 23:105–182

Shannon LV (2001) Benguela Current. Encyclopedia of Ocean Sciences 316–327 https://doi.org/10.1016/B978-012374473-9.00359-3

Souza JMA, de Boyer Montégut C, Le Traon PY (2011) Comparison Between Three Implementations of Automatic Identification Algorithms for the Quantification and Characterization of Mesoscale Eddies in the South Atlantic Ocean. Ocean Sci 7:317–334. https://doi.org/10.5194/os-7-317-2011

Stetsjuk GA (1983) Seasonal location of upwelling zones in ICSEAF Divisions 1.3,1.4 and 1.5,1.6 based on mean time series data. Collect Sci Pap 10(2) 173–178

Stewart RH (2006) Introduction to Physical Oceanography. Dept of Oceanogr, Texas A & M University

Svansson A (1975) Interaction between the coastal zone and the open sea. Finnish Mar Res 239:11–28

Travkin VS, Akhtyamova AF (2023) Spatial variability of the frontal zones and its eddies generated in the Norwegian Sea. Russ J Earth Sci, 23, ES3004. https://doi.org/10.2205/2023es000844

Udalov A, Budyansky M, Prants S (2023) A census and properties of mesoscale Kuril eddies in the altimetry era. Deep-Sea Research I 200:104129. https://doi.org/10.1016/j.dsr.2023.104129

van Sebille E, Griffies SM, Abernathey R et al (2018) Lagrangian ocean analysis: Fundamentals and practices. Ocean Model 121:49–75. https://doi.org/10.1016/j.ocemod.2017.11.008

Walin G (1972) Some observations of temperature fluctuations in the coastal region of the Baltic. Tellus 24:187–198

Woodson CB, Eerkes-Medrano DI, Flores-Morales A, Foley MM, Henkel SK, Hessing-Lewis M, Jacinto D, Needles L, Nishizaki MT, O'Leary J, Ostrander CE, Pespeni M, Schwager KB, Tyburczy JA, Weersing KA, Kirincich AR, Barth JA, McManus MA, Washburn L (2007) Local diurnal upwelling driven by sea breezes in northern Monterey Bay. Cont Shelf Res 27:2289–2302. https://doi.org/10.1016/j.csr.2007.05.014

Wysokinski A (1986) The living marine resources of the South-east Atlantic. University of Virginia, Food and Agriculture Organization of the United Nations